International Journal of Nanomedicine Dovepress

Open Access Full Text Article ORIGINAL RESEARCH

Stimuli-Responsive Peptide/siRNA Nanoparticles as a Radiation Sensitizer for Glioblastoma Treatment by Co-Inhibiting RELA/P65 and EGFR

Bohong Cen[1,2], Jian Zhang[1], Xinghua Pan[3], Zhongyuan Xu[2], Rong Li[1], Chengcong Chen[1], Baiyao Wang[1], Zhiyong Li[4], Guoqian Zhang[1], Aimin Ji[5], Yawei Yuan[1]

[1]Department of Radiation Oncology, Guangzhou Institute of Cancer Research, The Affiliated Cancer Hospital, Guangzhou Medical University, Guangzhou, Guangdong, 510095, People's Republic of China; [2]Clinical Pharmacy Center, Nanfang Hospital, Southern Medical University, Guangzhou, Guangdong, 510515, People's Republic of China; [3]Department of Biochemistry and Molecular Biology, School of Basic Medical Sciences, Southern Medical University, and Guangdong Provincial Key Laboratory of Single Cell Technology and Application, Guangzhou, Guangdong, 510515, People's Republic of China; [4]Department of Neurosurgery, Nanfang Hospital, Southern Medical University, Guangzhou, Guangdong, 510515, People's Republic of China; [5]Department of Pharmacy, The Seventh Affiliated Hospital of Southern Medical University, Foshan, Guangdong, 528244, People's Republic of China

Correspondence: Yawei Yuan; Aimin Ji, Email yuanyawei@gzhmu.edu.cn; aiminji_007@163.com

Purpose: To develop a novel approach for increasing radiosensitivity in glioblastoma (GBM) by using targeted nanoparticles to deliver siRNA aimed at silencing the EGFR and RELA/P65 genes, which are implicated in radioresistance.

Patients and Methods: We engineered biodegradable, tumor-targeted, self-assembled, and stimuli-responsive peptide nanoparticles for efficient siRNA delivery. We evaluated the nanoparticles' ability to induce gene silencing and enhance DNA damage under radiation in vitro and in vivo. The nanoparticles were designed to exhibit pH-responsive endosomal escape and αvβ3 integrin targeting, allowing for preferential accumulation at tumor sites and traversal of the blood-brain tumor barrier.

Results: The application of these nanoparticles resulted in significant gene silencing, increased apoptosis, and decreased cell viability. The treatment impaired DNA repair mechanisms, thereby enhancing radiosensitivity in GBM cells. In a GBM mouse model, the combination of nanoparticle treatment with radiotherapy notably prolonged survival without apparent toxicity.

Conclusion: Our findings suggest that nanoparticle-mediated dual gene silencing can effectively overcome GBM radioresistance. This strategy has the potential to improve clinical outcomes in GBM treatment, proposing a promising therapeutic avenue for this challenging malignancy.

Keywords: glioblastoma, siRNA delivery, self-assembly nanoparticles, radiation sensitizer

Introduction

Glioblastoma (GBM) is the most prevalent and devastating form of primary brain cancer, currently accounting for 50.9% of all malignant central nervous system tumor.[1] It is highly invasive and prone to recurrence, with a poor prognosis: a median survival time of less than 15 months and a 5-year survival rate of only 3–4%.[1,2] Radiotherapy is the standard and main curative treatment for GBM, which is commonly used to treat the vast majority of patients.[3] However, because of the heterogeneity of GBM, it is easy to develop adaptive radiotherapy resistance.[4] Although increasing the radiation dose in GBM treatment may improve survival rates, it also poses the risk of damaging healthy brain tissue by exposing normal cells to levels of radiation beyond their tolerance limit.[5] Thus, the primary focus of radiation oncology is to find an efficient strategy that promotes GBM radiosensitization by enhancing the effectiveness of radiation therapy, while minimizing damage to healthy cells.[6]

GBM cells develop radiation-resistant phenotypes due to genetic alterations during radiation therapy, leading to a low cure rate and poor prognosis.[4,7] DNA damage repair response (DDR) plays a crucial role in the development of radiation resistance by removing toxic DNA lesions to prevent genomic destabilization.[8] DDR processes include DNA damage

Received: 18 June 2024
Accepted: 4 November 2024
Published: 9 November 2024

detection, initiation of DNA repair, regulation of cell cycle, and apoptosis.[9] DDR system repairs double-strand breaks (DSBs) induced by ionizing radiation using two pathways: high-fidelity homologous recombination (HR) mediated by the Ataxia Telangiectasia-Mutated gene (ATM), and error-prone non-homologous end joining (NHEJ) mediated by DNA-dependent protein kinase (DNA-PK).[10] Both pathways repair DSBs induced by radiotherapy. HR occurs in S-G2 phase cells, while G0-arrested cells rely predominantly on NHEJ, in which HR is inactive.[10] Enhanced DDR may reduce the radiosensitivity of GBM and promote the development of radiation resistance in GBM.[11]

Radiation activates the EGFR/PI3K/Akt signaling pathway in a ligand-independent manner, promoting NHEJ repair of DSBs via promoting DNA-PK transcription and phosphorylation activation of genes.[12,13] Repeated irradiation can also activate the NF-κB signaling pathway abnormally, leading to HR repair in GBM and contributing to radiation resistance.[14] The activated NF-κB pathway can activate HR-related genes such as ATM, BRCA2, and CHK2, to repair DSBs, causing a decrease in tumor radiosensitivity.[14–16] Meanwhile, the activated NF-κB pathway can indirectly activate the c-Met pathway, promoting tumor cell survival.[17] Furthermore, NF-κB-dependent signaling can induce a mesenchymal state in proneural glioblastoma stem cells (GSCs), leading to increased radioresistance.[15] These mechanisms increase the DNA damage repair capacity and cell viability of tumors. Therefore, we developed radiosensitizers for GBM that inhibit both the EGFR and NF-κB pathways, co-inhibiting HR and NHEJ-mediated DSB repair and cell survival, thus effectively overcoming the problem of radiotherapy resistance in GBM.

RNA interference (RNAi) using siRNAs offers a promising approach for cancer therapy by silencing disease-related genes.[18,19] In 2018, ONPATTRO® (patisiran, ALN-TTR02) became the first siRNA therapeutic agent to receive approval from the United States Food and Drug Administration (FDA) and European Commission (EC) for treating hereditary transthyretin amyloidosis (hATTR) with polyneuropathy in adults, which officially declared that RNAi therapy has come from theory to reality.[20] Since then, the FDA has approved several other siRNA drugs. Compared to small molecule inhibitors and antibodies, siRNA can avoid drug resistance caused by protein structure mutations because it can completely base pair with conserved mRNA regions of target genes.[21,22] However, effective delivery of siRNAs to target cells remains challenging due to their hydrophilic nature, high molecular weight, and anionic charges.[23] To facilitate in vivo application of siRNA, it is crucial to address physiological and biological challenges including nuclease degradation, immune system recognition, clearance by the liver and kidneys, and tissue-specific targeting.[23] Although chemical modification of siRNA can address issues such as stability, immunogenicity, and non-specific effects, the development of appropriate delivery systems is necessary to achieve targeted delivery of siRNA to specific tissues or cells.[24] Peptide-based nucleic acid nanoparticles are favored among various non-viral gene delivery systems because of their biocompatibility, biodegradability, targeting ability, low cost, and easy preparation.[25] These self-assembled polymeric nanoparticles are formed by electrostatic adsorption, hydrogen bonding, or Van der Waals forces between siRNA molecules and oligopeptides.[25] However, functional modification is still required to achieve effective in vivo uptake by target cells and escape from endosomes after internalization.

Studies have suggested that surface PEGylation of polymer nanoparticle complexes can enhance their in vivo circulation time, allowing for increased delivery to targeted tissues.[26] However, the efficiency of siRNA entering the cytoplasm after endocytosis is a critical determinant of RNA interference activity.[23] Several mechanisms have been proposed for endosomal escape, including the proton sponge effect, which induces osmotic swelling through a high density of positive charges, but may lead to rapid clearance by the reticuloendothelial system due to concerns regarding distribution and half-life of nanoparticles.[23,27] Other mechanisms include membrane fusion and endosomal pore or channel formation, but each comes with limitations in terms of efficiency, incomplete release of endosomal contents, lack of cell specificity or difficulty applying to peptide/nucleic acid nanoparticles.[23,26,28] Additionally, directly targeting this activation to the cell membrane may cause significant cytotoxicity.[26] However, using intracellular-specific activation within the endosome could be an effective approach to address this issue.[26] In our research, we have developed a novel PEGylated peptide material that can activate specifically within endosomes to disrupt the endosomal membrane, thereby enhancing the release of siRNA into the cytoplasm. This approach offers the potential to reduce cytotoxicity while maximizing the effectiveness of the RNAi therapy.

The blood-brain tumor barrier (BBTB) is a key histopathological feature of glioblastoma that results from the formation of new blood vessels and integration of pre-existing brain capillaries into the tumor tissue.[29,30] This creates

a barrier with vessels possessing specific pore sizes and permeability, while still retaining some functions of the blood-brain barrier.[29] Integrin αvβ3 receptors are highly expressed on both neovascular endothelial cells and tumor cells in glioblastoma, and play a crucial role in tumor invasion and metastasis.[31] Cyclic RGD peptides can be used as targeting agents to exploit this characteristic and achieve brain-targeted delivery of drugs across the blood-tumor barrier, using receptor-mediated endocytosis and membrane trafficking for glioblastoma therapy.[32,33] Currently, there are 70 registered clinical trials for tumor tracers or targeted drugs based on cyclic peptide RGD in the US FDA clinical trial center, and 6 of these clinical trials are related to glioblastoma. These results demonstrate the potential clinical application of cyclic peptide RGD as a specific targeting agent for glioblastoma. Therefore, RGD-based delivery systems show significant potential in the treatment of GBM.

Animal models, particularly murine models of malignant glioma, are widely used to study the pathophysiology of GBM and to evaluate potential therapeutic strategies.[33,34] These models are considered valid for preclinical studies due to their ability to mimic the human disease in terms of tumor growth, invasion, and response to treatments.[35] In this research, we developed a novel peptide/nucleic acid nanoparticle platform by self-assembling siRNAs with (LLHH)3-Acp-2[mini-PEG]-GRRRRRRRRRG-2[mini-PEG]-Acp-cRGD peptide (cRGD-GR9G-(LLHH)3). This construct demonstrates the capacity to co-deliver siRNAs targeting EGFR and RELA/P65 genes to glioblastoma multiforme (GBM) cells with high efficiency, negating the requirement for invasive surgical interventions. The characterization and functional validation of these nanoparticles were conducted via evaluation of gene-silencing efficacy in both in vitro and in vivo models. Furthermore, this study explored the synergistic potential of the nanoparticles with conventional focused radiotherapy, resulting in enhanced radiosensitivity of GBM cells. The cellular uptake and intracellular release mechanisms, as well as the toxicity profile including hemotoxicity of the nanoparticles upon in vivo administration, were thoroughly assessed. The primary objective is to forge potent, low-toxicity radiosensitizers that target GBM, and also providing a robust theoretical and experimental basis for the integration of EGFR and NF-κB pathway inhibitors in radiotherapeutic strategies.

Materials and Methods

Reagents and Materials

U87MG cells line (human malignant glioblastoma multiforme cell line, ATCC Number: HTB-14) and U251MG (human malignant glioblastoma multiforme cell line, Serial Number: TCHu 58) was purchased from the Cell Bank of Type Culture Collection of the Chinese Academy of Sciences (Shanghai, China). The U87MG-Luc cell line was generated in our laboratory through transfection with a reporter gene encoding firefly luciferase, as previously reported.[36] The cells were cultured using DMEM supplemented with 10% FBS (Gibco, CA, USA), and were grown in a humidified atmosphere of 5% CO_2 at 37°C.

GRRRRRRRRRG-$CONH_2$, GRRRRRRRRRG-2[miniPEG]-Acp-cRGD, (LLHH)3-Acp-2[mini-PEG]-GRRRRRRRRRG-$CONH_2$, (LLHH)2-Acp-2[mini-PEG]-GRRRRRRRRRG-2[mini-PEG]-Acp-cRGD, (LLGG)3-Acp-2[mini-PEG]-GRRRRRRRRRG-2[mini-PEG]-Acp-cRGD and (LLHH)3-Acp-2[mini-PEG]-GRRRRRRRRRG-2[mini-PEG]-Acp-cRGD were synthesized by Guoping Pharmaceutical Co., LTD (China). siRNA sequences and modifications for this study were as follows: Human EGFR siRNA (siEGFR): Sense (5′-3′): (fC)(mC)(fU)UAGACUUACUUUU(fG)(mU)(fA), Antisense (5′-3′): P-(mU)(fA)(mC)AAAAGUAAGUCUA(mA)(fG)(mG)dTdT. human RELA/P65 siRNA (siP65): Sense (5′-3′): (fG)(mC)(fU)GCAGUUUGAUGAU(fG)(mA)(fA), Antisense (5′-3′): P-(mU)(fU)(mC)AUCAUCAAACUGC(mA)(fG)(mC)dTdT. Negative control siRNA (siNC): Sense (5′-3′): (fA)(mU)(fG)UAUUGGCCUGUAU(fU)(mA)(fG), Antisense (5′-3′): P-(mC)(fU)(mA)AUACAGGCCAAUA(mC)(fA)(mU)dTdT. mN represented 2′-O-methyl sugar-modified RNA nucleosides. fN represented 2′-fluoro sugar-modified RNA nucleosides. Indodicarbocyanine-5 (Cy5)-labeled siRNA (siRNA-Cy5) and all of the abovementioned siRNAs were synthesized from Guang-zhou RiboBio Co., Ltd. (China).

RNAiso Plus, SYBR® Premix Ex TaqTM and PrimeScriptTM RT reagent Kit with gDNA Eraser were from TaKaRa (Japan). Opti-MEM, Dulbecco's Modified Eagle's Medium (DMEM) and fetal bovine serum (FBS) were from Thermo Fisher Scientific (Massachusetts, USA). D-Luciferin was from Bioworld Technology (Minnesota, USA). ELISA kits

were from Mlbio (Shanghai, China). Antibody for Ki67 (ARG53222) was obtained from Arigo biolaboratories (China). Antibody for Phospho-Histone H2A.X (9718), Phospho-EGF Receptor (3777), EGF Receptor (4267), ATM (2873), Phospho-ATM (13050), NF-κB p65 (8242), Phospho-NF-κB p65 (3033) were obtained from Cell Signaling Technology (Danvers, MA). Antibodies for DNA PKcs (ab32566), and phospho-DNA PKcs (ab18192) were obtained from Abcam (Cambridge, UK). Antibodies for GAPDH (HRP-60004) were obtained from Proteintech Group (China). Anti-Human EGFR eFluor 660-conjugated antibody (50-9509-42) was from eBioscience (California, USA). Annexin V-FITC/PI apoptosis detection kit was obtained from KeyGEN biotech (China). CometAssay kit (4250-050-K) was obtained from Bio-Techne (Minnesota, USA). LysoTracker Green DND-26 (MB6042) was obtained from Meilunbio (China). Hoechst 33342 Stain solution (C0030) was obtained from Solarbio (China).

Synthesis, Purification and Characterizations of Peptides

All peptides, including GRRRRRRRRRG-$CONH_2$, GRRRRRRRRRG-2[miniPEG]-Acp-cRGD, (LLHH)3-Acp-2[mini-PEG]-GRRRRRRRRRG-$CONH_2$, (LLHH)2-Acp-2[mini-PEG]-GRRRRRRRRRG-2[mini-PEG]-Acp-cRGD, (LLGG)3-Acp-2[mini-PEG]-GRRRRRRRRRG-2[mini-PEG]-Acp-cRGD, and (LLHH)3-Acp-2[mini-PEG]-GRRRRRRRRRG-2[mini-PEG]-Acp-cRGD, were synthesized using solid-phase peptide synthesis (SPPS) with Fmoc (9-fluorenylmethyloxycarbonyl) chemistry. The synthesis was performed on a Liberty-12-Channel Automated Peptide Synthesizer equipped with an integrated microwave system, manufactured by CEM Corporation, USA. This equipment facilitates rapid and efficient coupling of amino acids, enhancing the purity of the synthesized peptides. The entire synthesis process was conducted by Guoping Pharmaceutical Co., LTD (China), ensuring high-quality peptide production for our research purposes. Peptides were purified by reversed-phase high-performance liquid chromatography (HPLC) using a C8 column (Waters, USA) and a gradient of ac etonitrile and deionized (DI) water containing 0.1% (v/v) TFA. Molecular weights (MWs) of peptides were analysed by matrix-assisted laser desorption/ionization time-of-flight mass spectrometry (MALDI-TOF-MS; BrukerReex, BrukerDaltonics, Inc., CA, USA).

Peptide solutions were prepared at a concentration of 50 μmol/L in a 50% trifluoroethanol/PBS (v/v) mixture to simulate the cell membrane environment (pH 7.4). The pH was adjusted to 6.0 using phosphoric acid to mimic the acidic environment of the endosome. The secondary structures of the complexes were analyzed using circular dichroism (CD) spectra recorded on a JASCO J-810 spectropolarimeter (Jasco, Inc., Eastern, Md, Japan). The spectra were obtained at 0.1 nm intervals ranging from 260 to 190 nm, using a 0.1 mm quartz cuvette. After subtracting the background, all spectra were normalized to a standard scale. The resulting curves were smoothed applying the spectropolarimeter's standard smoothing parameters.

Characterizations of Peptide and Nanoparticles

Lyophilized powder of peptides were resuspended in double-distilled water (ddH_2O) to prepare solutions of various concentrations. In a similar fashion, siRNAs were dissolved in RNase-free ddH_2O to obtain a final concentration of 8 μM. Peptides and siRNA were mixed according to different ratios (peptide/siRNA = weight/mol) of 0:1, 2:1, 4:1, 6:1, and 8:1 and incubated for 30 min at room temperature which was allowing for efficient siRNA encapsulation. Once completed, the preparations were ready for the next stages of the experimental process.

Agarose gel electrophoresis (AGE) was used to screen the best weight ratio of peptides to adsorb siRNA. Complexes formulated at various ratios were mixed with 6x DNA loading buffer and then subjected to electrophoresis on a 1.2% agarose gel that was pre-stained with GelstainRed (Catalog number: S2009L, UElandy, China). Electrophoresis was performed at 120 mV for 30 minutes. Following electrophoresis, the gels were examined and photographed under ultraviolet light. Naked siRNA served as a control for comparison in these experiments. Additionally, the particle size and zeta potential of the complexes at these different ratios were determined using dynamic light scattering (DLS) with a Malvern Zetasizer (Nano-ZS90, Malvern Instruments Ltd., Malvern, UK). The morphology of the nanoparticles were observed using a transmission electron microscope ([TEM] JEM-100CXII; JEOL, Tokyo, Japan).

Serum Stability and Hemolysis Analysis

The serum stability of the nanoparticles was assessed by incubating them with 50% fetal bovine serum at 37°C for 1, 3, 6, and 12 hours. The integrity of the complexes was evaluated using gel electrophoresis, and the release of siRNA was quantified. Distilled water was used as a negative control, and SDS was used as a positive control for degradation.

The hemolytic activity of cRGD-GR9G-(LLHH)3/siEGFR/siP65 nanoparticles was quantified by incubating them with rabbit erythrocytes at various concentrations for 3 hours at 37 °C, followed by vortexing. Rabbit blood was used to evaluate the hemolysis induced by cRGD-GR9G-(LLHH)3/siEGFR/siP65. Distilled water (H_2O) served as the positive control for hemolysis, while saline solution (NS) was used as the negative control.

Cellular Uptake and Intracellular Distribution

Cells were transfected with varying concentrations of different peptide/siEGFR-Cy5/siP65-Cy5 nanoparticles or a mixture of siEGFR-Cy5/siP65-Cy5 in Opti-MEM for 6 hours at 37°C. For the cellular uptake assay, cells were rinsed thrice with phosphate-buffered saline (PBS) to remove extracellular molecules. Subsequently, cells were digested with trypsin, washed twice with PBS, and resuspended in 0.1 mL of PBS. Fluorescence data were gathered using a FACS Verse flow cytometer (BD Biosciences, USA) and analyzed with Cell Quest software.

In the case of the confocal fluorescence microscopy assay, cells were transfected with different peptide/siEGFR-Cy5 /siP65-Cy5 nanoparticles or a mixture of siEGFR-Cy5/siP65-Cy5 at a concentration of 200 nM. After transfection, cells were washed with PBS. Cell nuclei were counterstained with Hoechst 33342 (blue), siRNA was labeled with Cy5 (red), and the endosome was labeled with LysoTracker Green DND-26 (green). Observations were made using confocal microscopy (Zeiss LSM 800, Germany).

Establishment of in vitro Assay

The cells were seeded into a variety of dishes (Corning, California, USA) at a predetermined density and allowed to attach for 24 hours. siNC, devoid of silencing capability, acted as a negative control. The treatment protocols for the respective groups were as follows: the control group received identical handling to the other groups except for the omission of any treatment; cRGD-GR9G-(LLHH)3/siNC; cRGD-GR9G-(LLHH)3/siEGFR; cRGD-GR9G-(LLHH)3/siP65; cRGD-GR9G-(LLHH)3/siEGFR/siP65; each was incubated with the cells for 6 hours in serum-free Opti-MEM. Subsequently, the Opti-MEM was supplanted by DMEM supplemented with 10% FBS, and the cells were further incubated for 48 hours, followed by 5 Gy of irradiation exposure. Post-irradiation, cells were subjected to incubation periods tailored to the specific assays being performed. The impact of irradiation on cells was evaluated using a suite of techniques. Clonogenic survival assays were conducted, and representative images of the cells were obtained. Flow cytometry was employed to measure apoptosis at 48 hours after treatment. Additionally, the comet assay was utilized to assess cellular damage, with images captured at 24 hours post-treatment.

RT-qPCR, Western Blot and Flow Cytometry for Target Gene Analysis

The RT-qPCR, flow cytometry and Western blot analysis were conducted as previously described.[33] The primer sequences for RT-qPCR analysis used in this experiment were as follows: Human P65/RELA (Forward primer: 5′-ATGTGGAGATCATTGAGCAGC-3′, Reverse primer: 5′-CCTGGTCCTGTGTAGCCATT-3′). Human EGFR (Forward primer: 5′-GCCGCAAAGTGTGTAACGGAATAG-3′, Reverse primer: 5′-TGGATCCAGAGGAGGAGTATGTGT-3′). Human GAPDH (Forward primer: 5′-CGGAGTCAACGGATTTGGTCGTAT-3′, Reverse primer: 5′-AGCCTTCTC CATGGTGGTGAAGAC-3′).

Clonogenic Survival Assay, Cell Apoptosis and Comet Analysis

For the Clonogenic Survival Assay, to evaluate cell survival post-radiation, a clonogenic assay was performed. Following radiation treatment, cells were seeded, allowed to grow to form colonies, and then stained with crystal violet. For cell apoptosis analysis, apoptosis was measured using an Annexin V-FITC/PI apoptosis detection kit according to the manufacturer's instructions. The rates of cell apoptosis were analyzed using a FACSverse flow cytometer. For the

Comet Assay, post-radiation DNA damage was assessed through the comet assay. Cells were embedded in agarose, lysed, electrophoresed, and stained with ethidium bromide. DNA damage was quantified by analyzing the tail length and DNA percentage in the tail, with representative images captured.

Intracranial Orthotopic Glioblastoma Model Establishment

Female nude mice (4–6 weeks old) were provided by the laboratory animal center of Southern Medical University. All animal studies were under the guidelines of the National Institutes of Health of China for the care and use of laboratory animals. All animal studies were approved by the Institutional Animal Care and Use Committee of the Southern Medical University.

An intracranial orthotopic glioblastoma model was established to investigate bio-distribution and anti-tumor efficacy of nanoparticles, according to previously described method.[33,37] In summary, U87MG-Luc cells were prepared in ice-cold serum-free DMEM at a concentration of 3×10^5 cells per 3 μL and maintained on ice. Nude mice underwent anesthesia with chloral hydrate and were secured to a stereotaxic frame using ear bars. A 1-cm midline incision was made to expose the skull, followed by the creation of a burr hole 2 mm to the right of the bregma and 1 mm behind the coronal suture, utilizing a Dremel tool with a 1-mm tip. The syringe was positioned perpendicular to the skull surface and inserted into the previously drilled hole, where 3 μL of U87MG-Luc cells were carefully injected over a 2-minute period at a depth of 3 mm. After the injection, the needle was left in place for an additional minute before its cautious withdrawal. Tumor growth was subsequently monitored using an in vivo imaging system (IVIS Lumina II, Caliper, USA).

In vivo Distribution Assay

Mice bearing orthotopic U87MG-Luc glioblastoma were injected intravenously with 1 nmol/20g of siEGFR-Cy5/siP65-Cy5, GR9G/siEGFR-Cy5/siP65-Cy5, cRGD-GR9G/siEGFR-Cy5/siP65-Cy5, GR9G-(LLHH)3/siEGFR-Cy5/siP65-Cy5, cRGD-GR9G-(LLHH)2/siEGFR-Cy5/siP65-Cy5, cRGD-GR9G-(LLGG)3/siEGFR-Cy5/siP65-Cy5, cRGD-GR9G-(LLHH)3/siEGFR-Cy5/siP65-Cy5 at single doses, respectively. The subsequent bio-distribution of different molecules labeled with Cy5 was detected at 24 h and 48 h using the IVIS imaging system (in red Cy5 emission spectrum). Intracranial U87MG-Luc glioblastoma was detected at 48 h using the IVIS imaging system (in luciferase emission spectrum). Ex-vivo fluorescence imaging was performed for different major organs harvested from orthotopic U87MG-Luc glioblastoma-bearing mice at 48 hours after injection.

In vivo Anti-Tumor Effects and Survival Monitoring Assay

To assess in vivo antitumor efficacy, we established a study using mice with orthotopic U87MG-Luc glioblastomas and organized them into 10 groups, each consisting of four individuals. Treatment commenced upon tumor detection through IVIS luminescent imaging. The timeline began with the first nanoparticle dose administered intravenously, denoting day 0 and the initiation of disease progression monitoring. Fifteen days before this point, mice were inoculated with U87MG-Luc cells. Nanoparticle treatments were administered on days 0, 3, 6, and 9, while radiotherapy at 2 Gy/day targeted brain tumors on days 1 through 5 and 8 through 12. Tumor assessment via IVIS occurred on days 0, 3, 6, 9, and 11. The therapeutic agents included saline; cRGD-GR9G-(LLHH)3/siNC; cRGD-GR9G-(LLHH)3/siEGFR; cRGD-GR9G-(LLHH)3/siP65; and cRGD-GR9G-(LLHH)3/siEGFR/siP65 (all at 1 nmol/20g). Mice experiencing severe morbidity or mortality were euthanized humanely, and their brains were excised for histological analysis and Hematoxylin and Eosin (H&E) staining.

Immunogenicity Evaluation and Toxicity Assay

The serum concentrations of Interleukin 6 (IL-6), Interferon Beta (IFN-β), and Tumor Necrosis Factor Alpha (TNF-α) were determined using Enzyme-Linked Immunosorbent Assay (ELISA) kits per the instructions provided by the manufacturer (Shanghai Enzyme-linked, China). Potential hepatotoxicity and nephrotoxicity were evaluated during the in vivo anti-tumor assay by analyzing serum samples from participating subjects. Serum concentrations of alanine aminotransferase (ALT), aspartate aminotransferase (AST), creatinine (CREA), and urea were gauged using the

automated Chemray 240 Analyzer (Rayto, China), following the procedures stipulated in the manufacturer's guide. Light microscopy (Zeiss, Germany) was utilized to capture and record images at the microscopic level.

Statistical Analysis

The results were expressed as the mean ± standard error. Homogeneity-of-variance test was conducted first. Student's *t*-test or one-way analysis of variance was performed for statistical analysis. $P < 0.05$ were considered statistically significant.

Results

Design of Nanoparticles

As shown in Figure 1A, this study designed six candidate peptides with the aim of targeting glioblastoma using peptides that can carry nucleic acids and escape from endosomes within cells, which were synthesized by solid-phase synthesis using Fmoc chemistry (sequences in Figure 1A). The designed peptides contain several functional segments, including a siRNA binding segment, an endosome escape and nanoparticle core segment, a PEG linker and a targeting segment.

As shown in Figures 1B and S1A, we used Pymol software to visualize and minimize the spatial structure of the candidate peptides. A linear distribution pattern was observed for all peptides, suggesting an unimpeded, individual functionality of the R9 group, PEG linker, (LLHH)3 group, and cRGD group, as they were all distributed linearly without mutual interference. All peptides were purified and analysed by HPLC (purity ≥ 95%) and MWs of the peptides were confirmed by MALDI-TOF-MS (Figure S1B).

The amphipathic α-helical conformation possesses the capacity to perturb biological membranes, thereby enhancing the endosomal escape efficiency of peptide/siRNA complexes.[38] Nevertheless, the direct engagement of the amphipathic α-helical peptide with cellular membranes may provoke pronounced cytotoxic effects.[39] Hence, it is imperative to tailor peptides that selectively adopt the amphipathic α-helical structure within the intracellular milieu, ensuring the siRNA delivery is both efficacious and non-toxic. Circular dichroism spectroscopy, as depicted in Figure 1C, was employed to ascertain the emergence of the amphipathic α-helical conformation in candidate peptides at physiological pH 7.4 (akin to the cell membrane environment) and at the more acidic pH 6.0 (reflective of the endosome environment). Notably, at pH 6.0, peptides with the (LLHH)3 motif displayed a characteristic absorption peak around 220 nm, indicative of an amphipathic α-helical conformation, whereas at pH 7.4, such absorption peaks were absent. This differential behavior indicates that the peptides with a (LLHH)3 architecture are predisposed to folding into amphipathic α-helices under intracellular conditions, and not when exposed to the external cell membrane milieu, paving the way for the formulation of innovative, low-toxicity intracellular carriers.

The assembly mechanism of nanoparticles is depicted in Figure 1D, inferred from fundamental characteristics identified through TEM, DLS, and gel retardation assays. Under physiological conditions (pH 7.4), three repetitions of (LLHH)3 can spontaneously form the core of a nanoparticle due to the hydrogen bonding properties of the histidine residues, which act as hydrogen bond acceptors and donors with the neutral imidazole groups in the side chains of histidine, as well as the alkyl chain hydrophobicity of the leucine side chains.[28,40] The positively charged 9-arginine oligopeptide (R9) can form a weakly positive surface on the nanoparticle by combining with negatively charged siRNA, while PEG on the periphery of the nanoparticle increases hydrophilicity and tissue compatibility, in order to avoid nanoparticle aggregation, prolong in vivo circulation and reduce toxicity.[41] Surface-conjugated c(RGDfk)s oligopeptide groups can target the integrin αvβ3 receptors on the membrane of neovascular endothelial cells across the blood-brain barrier, and target the αvβ3 receptors on glioblastoma cells, achieving specific binding to tumor cells.[32,33] By means of this, the peptide and siRNA assembled into spherical nanoparticles with c(RGDfk)s displayed on their surface for the targeting of αvβ3 receptors.

This study introduces a nano delivery system based on the stimuli-responsive peptide cRGD-GR9G-(LLHH)3 for effective siEGFR and siP65 delivery, serving as a radiation sensitizer for glioblastoma in both in vitro and in vivo contexts. Figure 1E conceptually outlines the delivery mechanism of siEGFR/siP65 by cRGD-GR9G-(LLHH)3, where nanoparticles are endocytosed by cells and release their cargo into the cytoplasm following endosomal membrane

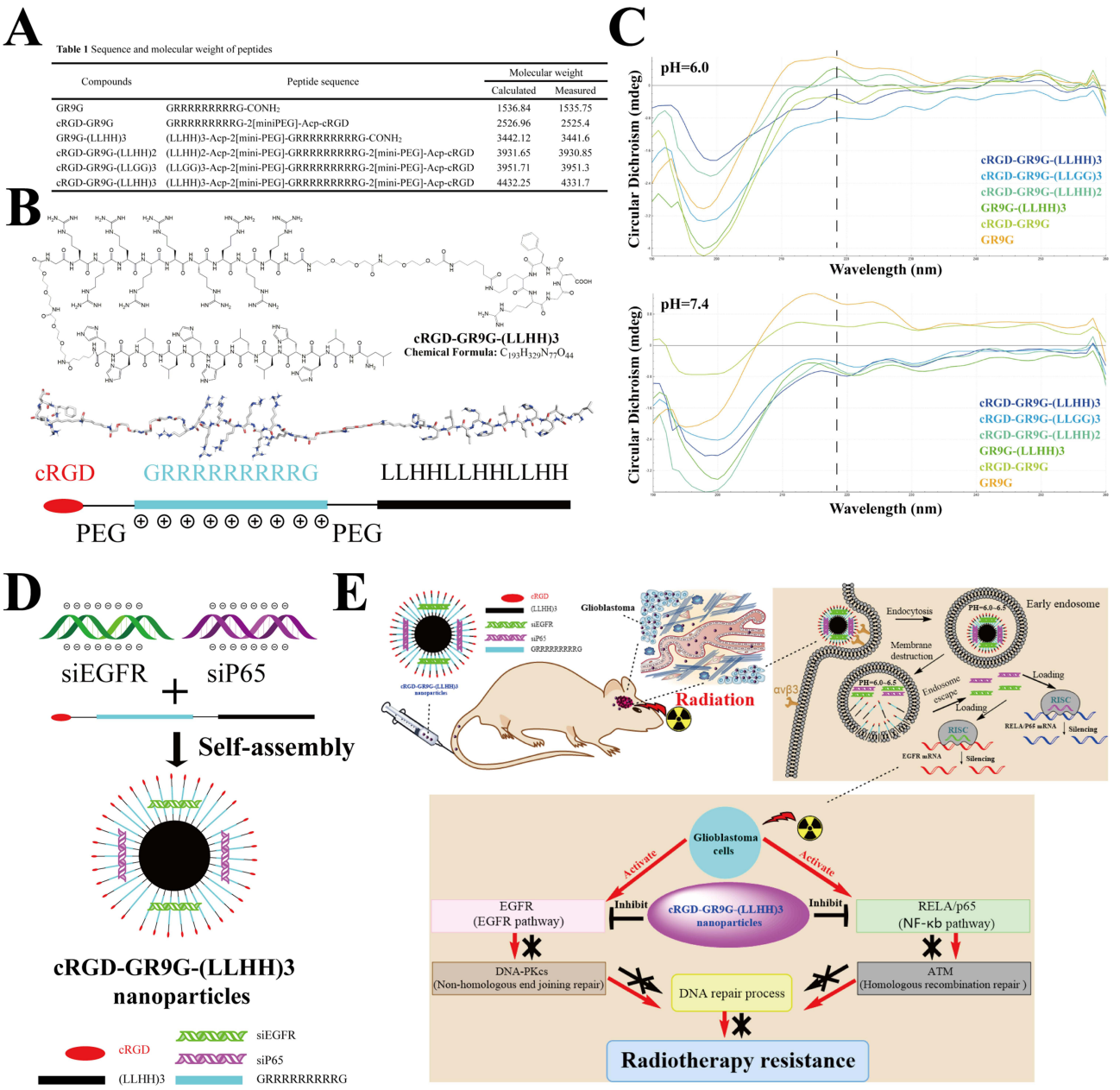

Figure 1 The schematic depiction and characterization of peptides and peptide/siRNA nanoparticle for targeted glioblastoma therapy. (**A**) Peptide designs and their molecular weights. (**B**) The chemical and stereochemical structure of (LLHH)3-Acp-2[mini-PEG]-GRRRRRRRRRG-2[mini-PEG]-Acp-cRGD peptide (cRGD-GR9G-(LLHH)3). (**C**) The circular dichroism spectra of the designed peptides at pH 6.0 and pH 7.4. (**D**) The mechanism for the formation of cRGD-GR9G-(LLHH)3/siRNA nanoparticle. (**E**) Schematic of co-delivering siEGFR and siP65 with nanoparticles facilitated by stimuli-responsive cRGD-GR9G-(LLHH)3 peptide as a radiation sensitizer for glioblastoma treatment.

disruption by the amphipathic α-helical structure of (LLHH)3. Subsequently, the siRNAs engage with the RNA-induced silencing complex (RISC), leading to the cleavage of messenger RNA (mRNA) and preventing the synthesis of EGFR and P65 proteins, thereby co-inhibiting RELA/P65 and EGFR.

Preparation and Characterization of Nanoparticles

To evaluate the ability of candidate peptides to protect siRNAs from degradation by serum nucleases and investigate the siRNA binding mechanism, the release of siRNAs from the peptide/siRNA nanoparticles were assessed by the gel retardation assay. The optimal peptide-to-siRNA ratio is essential for generating self-assembled nanoparticles that are

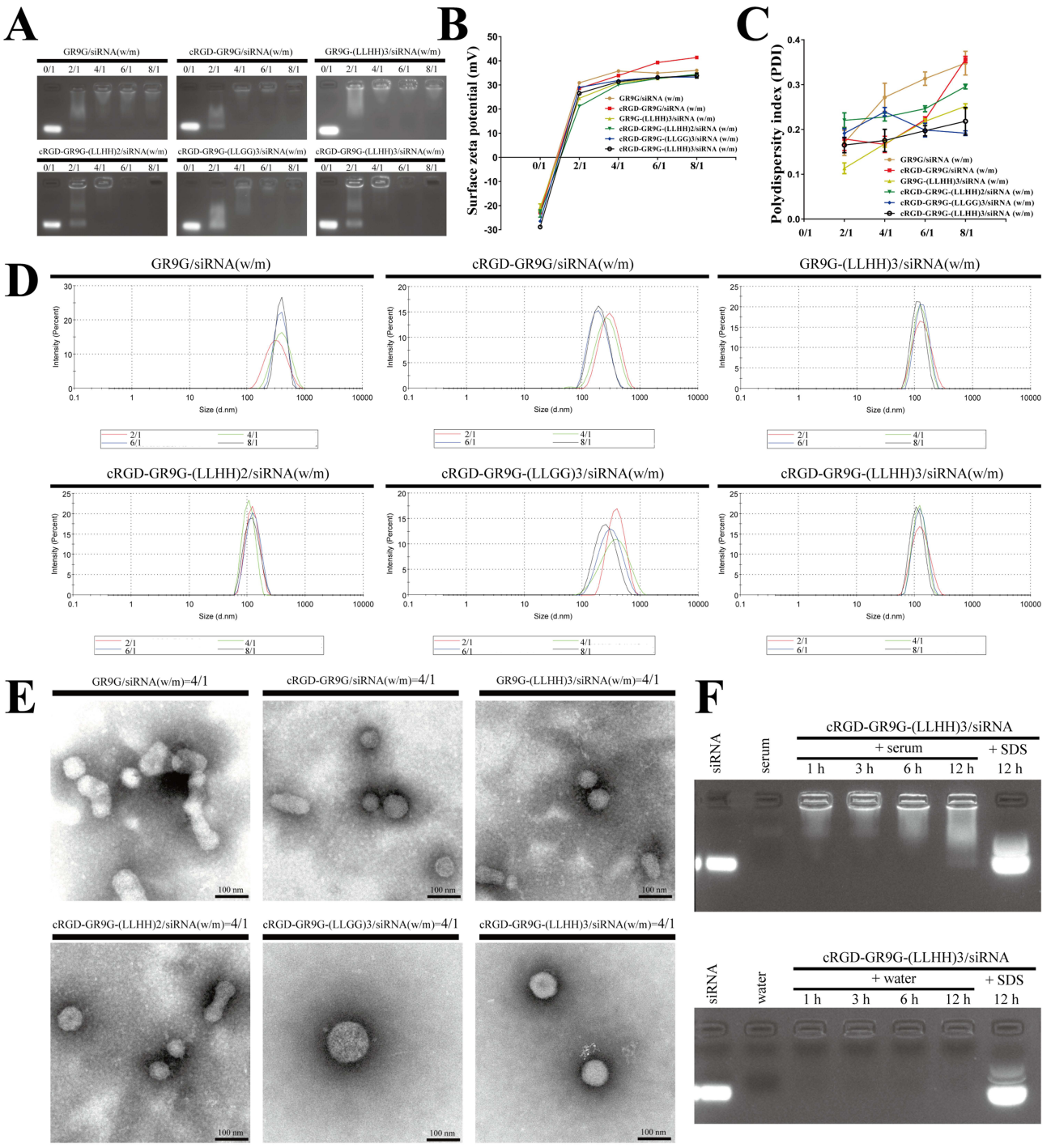

Figure 2 Characterizations of peptide/siRNA nanoparticles. (**A**) Gel electrophoresis image of peptide/siRNA complexes prepared at different ratios (peptide/siRNA = weight/ mol). Surface zeta potential (**B**), polydispersity index (**C**), particle size (**D**) and transmission electron microscope images (**E**) of peptide/siRNA complexes at different ratios. (**F**) Stability of cRGD-GR9G-(LLHH)3/siRNA complexes in serum. We examined the stability of cRGD-GR9G-(LLHH)3/siRNA (w/m = 6:1) complexes by incubating them with 10% FBS or water for 1, 3, 6, and 12 hours with 10% SDS as a positive control. Bar=100 nm.

uniform in size and have the desired particle size distribution. To this end, nanoparticles were synthesized at varying weight/molar ratios of peptide to siRNA. Figure 2A illustrates that increasing the peptide amount resulted in a higher retention of siRNAs within the nanoparticles. Notably, when the peptide-to-siRNA ratio surpassed 4, a significant majority of the siRNAs remained entrapped within the wells, suggesting that beyond this ratio, candidate peptides are capable of completely encapsulating siRNAs, thereby facilitating nanoparticle formation.

Studies have shown that exceeding a certain threshold for particle size can cause retention by the reticuloendothelial system in vivo, whereas reducing particle size can result in filtration and excretion by the kidneys.[42] In addition, if the surface potential is low, it may reduce binding to cells, affecting uptake and leading to nanoparticle aggregation, whereas high surface potential can cause non-specific binding with cells, leading to excessive toxicity.[43] Therefore, appropriate surface potential and particle size distribution are crucial for cellular uptake of nanoparticles. By measuring the surface zeta potential, polydispersity index, and particle size distribution (as shown in Figure 2B–D), it was found that when the ratio between peptide and siRNA exceeded 4, the resulting nanoparticles all showed a positive zeta potential, PDI below 0.3, and an average particle size of less than 200 nm. Interestingly, compared with other nanoparticles, the cRGD-GR9G-(LLHH)3/siRNA nanoparticles had the lowest PDI and the average particle size was around 100 nm. Transmission electron microscopy images (Figure 2E) showed that cRGD-GR9G-(LLHH)3/siRNA nanoparticles at a 4:1 ratio had uniform spherical shape and size. This implies that the particle size and surface potential of cRGD-GR9G-(LLHH)3/siRNA nanoparticles meet the minimum compatibility for cellular uptake requirements. Furthermore, backbone of siRNA was modified with 2′-O-methyl (2′-OMe) or 2′-Fluoro (2′-F) in recommended nucleotides to improve siRNA stability.

The stability evaluation of siRNA nanoparticles in vivo encompasses two primary considerations. Firstly, it is important to determine if siRNA is vulnerable to degradation by a range of nucleases present in the serum. Secondly, the potential for siRNA nanoparticles to dissociate in serum should be examined. Issues, such as siRNA degradation or leakage, could potentially obstruct its transport to the target site. As depicted in Figure 2F, we subjected the siRNA nanoparticles to various treatments (SDS as a positive control, deionized water as a negative control, and 10% FBS as an experimental group) and found that, within a 12-hour incubation period, the nanoparticles in the experimental group remained intact, resembling the negative control group. There was no dissociation or degradation observed in the pore, whereas siRNA leaked from the nanoparticles in the SDS-treated positive control group. This discovery indicates that, within a 12-hour timeframe, cRGD-GR9G-(LLHH)3/siRNA nanoparticles maintain stability in serum, a duration adequate for the nanoparticles to accumulate in the targeted tumour tissue.

In addition, we conducted gel retardation assays to assess siRNA release at different pH values. PBS was used to simulate the physiological environment (pH 7.4), while the pH was adjusted to 5.0 and 6.8 using phosphate buffer solution to mimic the acidic conditions of the endosome. As shown in Figure S5, our results show that siRNA release was minimal at physiological pH 7.4 but significantly increased at acidic pH levels of 5.0 and 6.8, confirming their pH-responsive behavior and ability to release siRNA under endosomal conditions.

Cellular Uptake, Intracellular Distribution, and Tumor Targeting of Nanoparticles in vitro and in vivo

To assess the cellular uptake and distribution of nanoparticles, siEGFR and siP65 were conjugated with the Cy5 fluorophore and self-assembled with peptides to generate nanoparticles. Cellular uptake of various peptide/siRNA nanoparticle formulations at differing concentrations was quantified using flow cytometry to determine the optimal concentration for maximal uptake and to explore the effect of nanoparticle structure on uptake efficiency.

In glioblastoma cells (U87MG and U251MG both expressed the integrin αvβ3 receptor shown in Figure S2C) treated directly with these nanoparticles, without auxiliary transfection agents, the cRGD-GR9G-(LLHH)3/siEGFR-Cy5/siP65-Cy5 formulation demonstrated a superior uptake rate of over 60% at 100nM, as delineated in Figures 3A and S2A. Conversely, nanoparticles lacking cRGD or containing modifications of the (LLHH)3 motif exhibited negligible uptake. These data suggest that the cRGD motif facilitates cellular uptake, while the (LLHH)3 structure promotes nanoparticle internalization. Cooperative function between these motifs is imperative for effective nanoparticle uptake. Furthermore, at 200nM, the uptake rate for the aforementioned nanoparticles surpassed 95%, prompting the use of this concentration in subsequent in vitro experiments.

To study cellular internalization and intracellular trafficking, glioblastoma cells (U87MG and U251MG) were treated with nanoparticles encapsulating siEGFR-Cy5 and siP65-Cy5. Subsequent to treatment, endosomes were stained with LysoTracker Green (emitting green fluorescence), and nuclei were counterstained with Hoechst 33342 (producing blue fluorescence). Fluorescence microscopy was performed 6 hours post-treatment to visualize nanoparticle uptake and

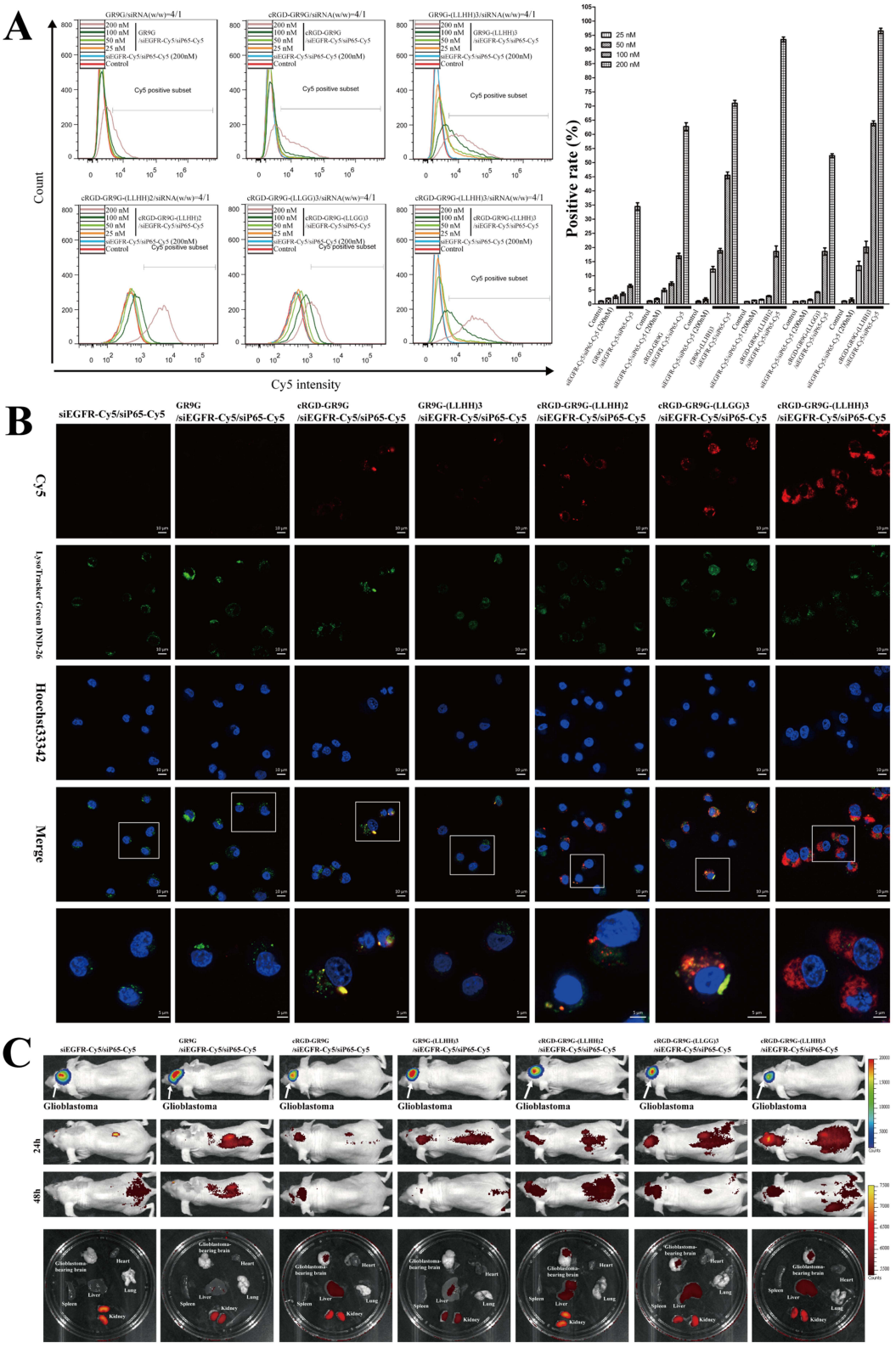

Figure 3 Cellular uptake, intracellular distribution and intracranial tumor permeability of peptide/siRNA nanoparticles in vitro and in vivo. Cellular uptake levels of different peptide/siEGFR-Cy5/siP65-Cy5 nanoparticles or siEGFR-Cy5/siP65-Cy5 mixture at different concentrations in U87MG cells incubated in Opti-MEM for 6 h at 37°C were measured by flow cytometry. (**B**) Confocal fluorescence microscopy images of intracellular distribution of different peptide/siRNA nanoparticles. U87MG cells were transfected with different peptide/siEGFR-Cy5/siP65-Cy5 nanoparticles or siEGFR-Cy5/siP65-Cy5 mixture incubated in Opti-MEM for 6 hours at 37°C. Cell nuclei were counterstained with Hoechst33342 (blue), siRNA was labeled with Cy5 (red) and endosome was labeled with LysoTracker Green DND-26 (green). (**C**) In vivo imaging of mice bearing orthotopic U87MG-Luc glioblastoma with different treatments. Mice were injected intravenously with 1 nmol/20g of different peptide/siEGFR-Cy5/siP65-Cy5

intracellular localization. As depicted in Figures 3B and S2B, a distinctive lack of colocalization between siRNA-Cy5 and LysoTracker Green signals was observed in cells treated with cRGD-GR9G-(LLHH)3/siEGFR-Cy5/siP65-Cy5 nanoparticles, indicating successful endosomal escape of siRNA-Cy5. In contrast, the fluorescence signals from siRNA-Cy5 in cells treated with other nanoparticle variants overlapped with LysoTracker Green, implying retention within the endosomes. These findings demonstrate that cRGD-GR9G-(LLHH)3/siRNA nanoparticles possess a unique capability for bypassing intracellular barriers, thereby facilitating efficient siRNA delivery and release within GBM cells.

To explore the biodistribution and intracranial tumor penetration of candidate nanoparticles in vivo, an orthotopic glioblastoma xenograft model with a luciferase reporter gene (U87MG-luc) was established. Nanoparticles, at a dosage of 1 nmol/20g, were intravenously administered to the mice. The in vivo distribution patterns were assessed with IVIS luminescent imaging at 24 and 48 hours after injection. Analysis of in vivo whole-animal and excised tissue fluorescence (Figure 3C) demonstrated that the nanoparticles predominantly accumulated in the kidneys, followed by the liver—the principal organs of elimination. Nanoparticles without a targeting moiety, notably siEGFR-Cy5/siP65-Cy5, GR9G/siEGFR-Cy5/siP65-Cy5, and GR9G-(LLHH)3/siEGFR-Cy5/siP65-Cy5, displayed no detectable tumor site fluorescence. Conversely, those containing the cRGD moiety, such as cRGD-GR9G/siEGFR-Cy5/siP65-Cy5, cRGD-GR9G-(LLHH)2/siEGFR-Cy5/siP65-Cy5, cRGD-GR9G-(LLGG)3/siEGFR-Cy5/siP65-Cy5, and particularly cRGD-GR9G-(LLHH)3/siEGFR-Cy5/siP65-Cy5, showed discernible tumor fluorescence, with the latter nanoparticle achieving the highest tumor retention. Our data indicate that the cRGD-GR9G-(LLHH)3/siEGFR-Cy5/siP65-Cy5, nanoparticles exhibit specific brain targeting, enhanced uptake by glioblastoma cells, and are predominantly cleared through hepatic and renal routes.

Enhancing Radiosensitivity with Nanoparticles: Effects on Clonogenicity, Apoptosis and DNA Repair in vitro

This study examined the radiosensitizing impact of nanoparticles on glioblastoma cells, assessing colony formation, apoptosis and DNA damage responses. Light microscopy disclosed post-radiation morphological alterations in both U87MG and U251MG cells (Figures 4A and S3A), including cell rounding and vacuolization, effects that were further enhanced by nanoparticle pre-treatment. Parallel evidence was obtained from the colony formation assays: achieving dual gene silencing of EGFR and P65 and coupling this with radiation treatment led to the total eradication of tumor cell colonies. The apoptosis assay depicted in Figure 4B demonstrated that radiation alone significantly induced apoptosis in U87MG cells, with an observed apoptosis rate of approximately 27.45%. This rate was notably higher compared to the 11.04% observed in the untreated control group. Furthermore, the cells exhibited an increased apoptotic response when pre-treated with nanoparticles that targeted both the EGFR and P65 genes, resulting in an apoptosis rate of 37.11%. A similar phenomenon was also observed in the apoptosis experiments with U251MG cells, as shown in Figure S3B. Conclusively, these findings collectively suggest that cRGD-GR9G-(LLHH)3/siEGFR/siP65 nanoparticles have the potential to significantly augment the efficacy of radiation therapy, primarily by stimulating apoptosis in glioblastoma cells.

This study assessed the capability of cRGD-GR9G-(LLHH)3/siEGFR/siP65 nanoparticles to enhance the cytotoxic effects of radiation therapy by promoting significant DNA damage in tumor cells. DNA fragmentation was evaluated using Comet assays 48 hours post-radiation exposure in U87MG cells (see Figure 4C). The results suggested that DNA damage caused by irradiation at 5 Gy, either unaccompanied or combined with control siRNA nanoparticles, was largely mitigated within the 48-hour period. However, a stark divergence was observed in cells subjected to radiation in conjunction with either EGFR or P65 gene silencing, which manifested as persisting DNA damage. Interestingly, cells under concurrent EGFR and P65 gene inhibition depicted the most pronounced increase in DNA fragmentation, reflected

nanoparticles or siEGFR-Cy5/siP65-Cy5 mixture at single doses. The subsequent bio-distribution of different molecules labeled with Cy5 was detected at 24 h and 48 h using the IVIS imaging system (in red Cy5 emission spectrum). Intracranial U87MG-Luc glioblastoma was detected at 48 h using the IVIS imaging system (in luciferase emission spectrum). Ex-vivo fluorescence imaging was performed for different major organs harvested from orthotopic U87MG-Luc glioblastoma-bearing mice at 48 hours after injection.

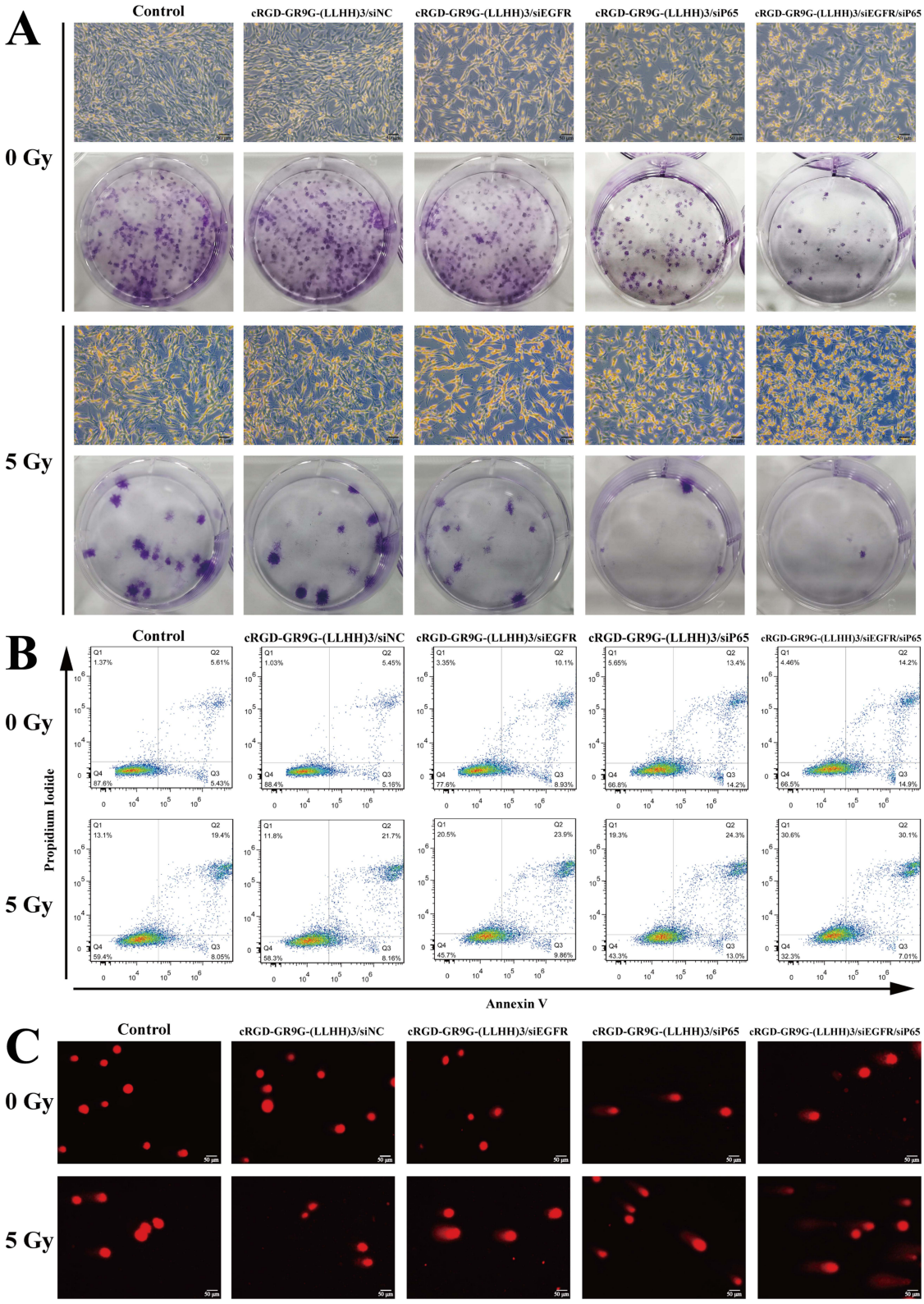

Figure 4 In vitro evaluation of the combined effect of radiation and cRGD-GR9G-(LLHH)3/siRNA on the clonogenic survival, apoptosis, and DNA damage of glioblastoma cells. The cells were treated with various cRGD-GR9G-(LLHH)3/siRNA nanoparticles in serum-free Opti-MEM for 6 hours. Subsequently, the Opti-MEM culture medium was replaced with 10% FBS/DMEM culture medium and cells were incubated for 48 hours, followed by exposure to 5 Gy radiation. The cells were then further incubated for a specific length of time, as per the assay requirements. The effects of radiation treatment on U87MG cells were assessed in the following ways: (**A**) Clonogenic survival assays were conducted on U87MG cells, and representative images were obtained. Bar=50 μm. (**B**) Apoptosis was analyzed using flow cytometry after 48 hours of treatment. (**C**) The comet assay was performed on U87MG cells, and representative images were captured after 24 hours of treatment.

by a surge in the DNA "tail" percentage. A similar phenomenon was also observed in the comet experiments with U251MG cells, as shown in Figure S3C. This highlights the compromised DNA repair capabilities of cells following radiation if these genes are suppressed. The amplified fragmentation through simultaneous EGFR and P65 inhibition corresponds with the predicted mechanism of NHEJ interruption via EGFR blockade and HR impediment through P65 repression.

Enhanced Radiosensitization Through Nanoparticle-Induced Gene Silencing and Disruption of DNA Repair Pathways in in vitro

This study analyzed the expression of EGFR and RELA/P65 genes in clinical glioblastoma samples and their association with DNA repair mechanisms by utilizing TCGA-GBM dataset for correlation analysis. Our analysis, illustrated in Figure 5A, indicates that both EGFR and RELA/P65 are markedly overexpressed in primary and recurrent GBM specimens relative to normal brain tissue. Additionally, the Gene Set Enrichment Analysis (GSEA) algorithm was employed to gauge the activity of gene sets related to NHEJ and HR DNA repair pathways in TCGA glioblastoma transcriptomes. Subsequently, we assessed the relationship between the activation of these pathways and the expression levels of EGFR and RELA/P65. The findings reveal a significant positive correlation between EGFR expression and NHEJ pathway activity, while RELA/P65 expression also displayed a significant positive correlation with NHEJ. Based

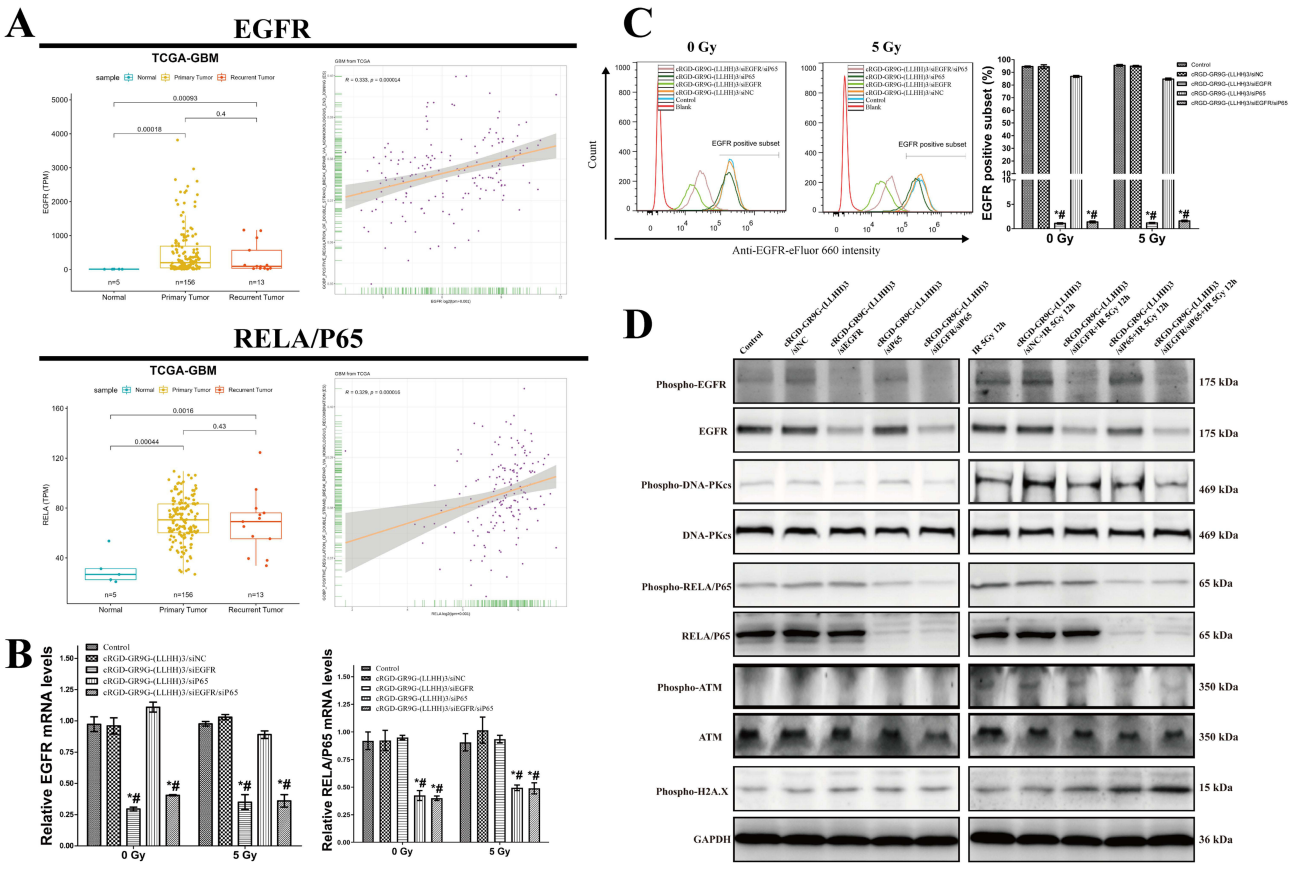

Figure 5 Mechanism of the effect of radiation combined with nanoparticles on increasing the radiosensitivity of glioblastoma cells in vitro. (**A**) Analysis of EGFR and RELA/P65 expression in normal tissue, primary tumor tissue, and recurrent tumor tissue using TCGA-GBM data, and the relationship between EGFR and GSEA scores of positive regulation of double strand break repair via nonhomologous end joining pathway, as well as the relationship between RELA/P65 and GSEA scores of positive regulation of double strand break repair via homologous recombination (ES) pathway. (**B**) Quantitative analysis of EGFR or RELA/P65 mRNA level using RT-qPCR after 48-hour treatment with nanoparticles (100 nM) or after treatment followed by exposure to 5 Gy radiation. The results were then normalized using GAPDH mRNA level. (**C**) Flow cytometry was used to analyze the EGFR expression after 48-hour treatment with nanoparticles (100 nM) or after treatment followed by exposure to 5 Gy radiation. (**D**) Western blot was performed to detect the expression levels of DNA repair pathway-related proteins (Phospho-EGFR, EGFR, Phospho-DNA-PKcs, DNA-PKcs, Phospho-RELA/P65, RELA/P65, Phospho-ATM, ATM, Phospho-H2A.X and GAPDH) in each treatment group (100 nM), with GAPDH used as an internal reference. *represents a comparison with the control group, P<0.05; # represents a comparison with the cRGD-GR9G-(LLHH)3/siNC group, P<0.05.

on the TCGA-GBM data, there is a strong implication that targeting EGFR and RELA/P65 could downregulate NHEJ and HR DNA repair pathways, offering a therapeutic avenue in glioblastoma treatment.

To elucidate the effect of cRGD-GR9G-(LLHH)3/siEGFR/siP65 nanoparticles on DNA repair in GBM cells, we initially assessed gene silencing efficacy in cells exposed to radiation. Data from 48-hour treatments indicated that, relative to comparison groups, these nanoparticles (100nM) substantially reduced EGFR and P65 gene expression in both irradiated and non-irradiated GBM cells, achieving over 75% silencing (Figure 5B). This implies the robustness of the nanoparticles' gene silencing capability notwithstanding radiation exposure. Flow cytometric analysis further demonstrated a pronounced reduction in EGFR membrane protein expression, especially in cells pretreated with 5Gy of radiation, resulting in up to 95% suppression (Figure 5C).

Utilizing Phospho-H2A.X as an indicator for DNA breaks, our study explored the contributions of EGFR, DNA-PKcs, RELA/P65, and ATM in the DNA repair processes through NHEJ and HR pathways. The expression and phosphorylation levels of these proteins were analyzed 12 hours following a subsequent 5Gy irradiation dose administered to GBM cells pre-treated with nanoparticles for 72 hours. The results (Figure 5D) indicated that, compared to the control group, there was no significant change in the Phospho-H2A.X levels in GBM cells after the 12-hour post-irradiation period. However, the phosphorylation levels of proteins associated with DNA break repair, such as Phospho-EGFR, Phospho-RELA/P65, Phospho-DNA-PKcs, and Phospho-ATM, were found to increase. This suggests that GBM cells undergo DNA double-strand breaks post-irradiation and activate related DNA repair pathways. Despite this, the broken DNA strands were essentially repaired after a 12-hour repair process, indicating an inherent capability of GBM cells for DNA repair and radiation resistance. cRGD-GR9G-(LLHH)3/siEGFR/siP65 nanoparticles aim to disrupt this repair mechanism, thereby enhancing the effectiveness of radiation therapy. Results (Figure 5D) confirmed that in combination with radiation, these nanoparticles significantly suppressed the expression of EGFR and P65 and markedly increased the level of Phospho-H2A.X, while reducing the levels of Phospho-DNA-PKcs and Phospho-ATM. Notably, radiation combined with cRGD-GR9G-(LLHH)3/siEGFR nanoparticles predominantly affected the NHEJ repair pathway, whereas radiation combined with cRGD-GR9G-(LLHH)3/siP65 nanoparticles chiefly impacted the HR repair pathway. Therefore, only by simultaneously inhibiting the EGFR and P65 genes can we effectively diminish the DNA double-strand break repair actions via NHEJ and HR pathways, thus enhancing the radiation-induced DNA damage in GBM cells.

Influence of Nanoparticles on Tumor Growth and Survival Time in Orthotopic Glioblastoma Mice and Its Evaluation of Immunogenicity and Toxicity

Previous experiments have shown that cRGD-GR9G-(LLHH)3/siEGFR/siP65 nanoparticles are readily taken up by GBM cells in vitro, where they escape endosomal entrapment and silence EGFR and P65 genes. This silencing significantly enhances the therapeutic efficacy of radiotherapy in eliminating tumor cells. Furthermore, the nanoparticles exhibit remarkable stability, with no evidence of dissociation or degradation after 12 hours in serum, as evidenced by Figure 2F. Moreover, they display no hemolytic when incubated with red blood cells, as demonstrated in Figure S4D, confirming their stability and non-hemolytic nature in vivo. To assess the combined effect of the nanoparticles and radiotherapy on glioblastoma in vivo, nude mice bearing orthotopic U87MG-Luc glioblastoma received four intravenous injections of the nanoparticles at three-day intervals, as shown in Figure 6A. The mice were also subjected to two cycles of daily radiotherapy, consisting of 2 Gy over five fractions, with a three-day hiatus between cycles. Tumor progression within the brain was tracked longitudinally using IVIS imaging at days 0, 5, and 11 following treatment initiation. After 15 days of therapy, mice were euthanized, and their brains, containing the glioblastoma, were harvested for imaging. Additionally, tissues from tumors, heart, liver, spleen, kidneys, and lungs were collected for histopathological examination.

As illustrated in Figure 6B and C, mice were categorized into two primary groups: normal controls and those subjected to radiotherapy. Within these groups, subdivisions were made to administer either saline (Control group), cRGD-GR9G-(LLHH)3/siNC (nanoparticles lacking gene silencing capabilities), cRGD-GR9G-(LLHH)3/siEGFR (nanoparticles targeting the EGFR gene for silencing), cRGD-GR9G-(LLHH)3/siP65 (nanoparticles targeting the

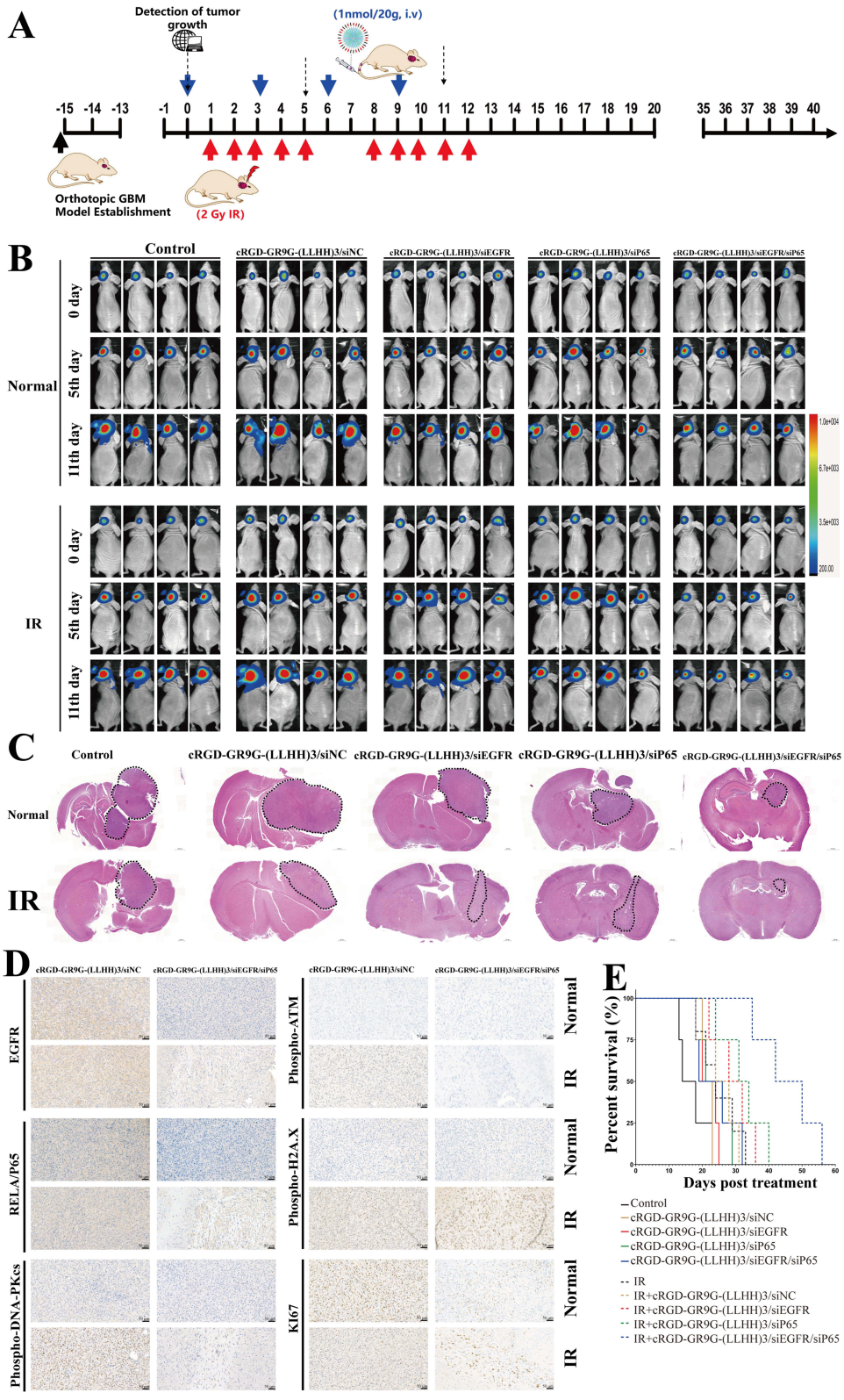

Figure 6 The anti-tumor effectiveness and mechanism of combining radiation and cRGD-GR9G-(LLHH)3/siRNA in an orthotopic U87MG-Luc glioblastoma model. (**A**) Schedule of tumor inoculation and treatment. The time frame of the experiment was established by considering the first treatment of nanoparticles administered via intravenous injection to the tumor-bearing mice as the starting point, with day 0 being marked as the beginning of the study to track the progression of the disease. Mice were injected orthotopically with U87MG-Luc cells at day-15. On days 0, 3, 6, and 9, the tumor-bearing mice were treated with nanoparticles. On days 1, 2, 3, 4, 5, 8, 9, 10, 11, and 12, the mice were treated with 2 Gy/day of radiotherapy for brain tumors. On days 0, 3, 6, 9, and 11, the tumors were monitored using IVIS. (**B**) IVIS luminescent imaging of glioblastoma-bearing mice. Conditions of the treatment were as follows: Control group (saline), cRGD-GR9G-(LLHH)3/siNC (1 nmol/20g) group, cRGD-GR9G-(LLHH)3/siEGFR (1 nmol/20g) group, cRGD-GR9G-(LLHH)3/siP65 (1 nmol/20g) group, or cRGD-GR9G-(LLHH)3/siEGFR/siP65 (1 nmol/20g) group. (**C**) When the

RELA/P65 gene for silencing), or cRGD-GR9G-(LLHH)3/siEGFR/siP65 (nanoparticles silencing both the RELA/P65 and EGFR genes). Results indicated that, following a 15-day treatment period, low-dose radiation marginally slowed tumor progression but failed to significantly eliminate tumor cells, revealing radioresistance and highlighting the potential benefit of combinational therapies for optimal glioblastoma eradication. No notable differences in tumor response were observed between the saline and cRGD-GR9G-(LLHH)3/siNC groups across both non-radiotherapy and radiotherapy cohorts, suggesting a lack of anti-tumor properties in cRGD-GR9G-(LLHH)3/siNC. In contrast, in the non-radiotherapy group, the cRGD-GR9G-(LLHH)3/siEGFR, cRGD-GR9G-(LLHH)3/siP65, and cRGD-GR9G -(LLHH)3/siEGFR/siP65 formulations all demonstrated tumor suppression, with the dual-gene silencing nanoparticles showing the most pronounced effect. Remarkably, within the radiotherapy group, the cRGD-GR9G-(LLHH)3/siEGFR/siP65 combination significantly outperformed the saline and cRGD-GR9G-(LLHH)3/siNC groups in inhibiting tumor growth. Nanoparticles targeting solely the EGFR or P65 gene modestly enhanced radiotherapy's efficacy. Furthermore, the synergistic application of radiotherapy and cRGD-GR9G-(LLHH)3/siEGFR/siP65 markedly improved glioblastoma cell eradication compared to the use of cRGD-GR9G-(LLHH)3/siEGFR/siP65 nanoparticles alone.

Studies on the mechanism by which in vivo nanoparticles enhance radiotherapy cytotoxicity revealed that, as shown in the immunohistochemical results in Figure 6D, compared to the non-radiotherapy group, residual tumor cells after radiotherapy treatment showed high expression of phospho-DNA-PKcs and phospho-ATM. This indicates that the remaining tumor cells can activate both NHEJ and HR repair pathways to repair double-strand breaks, which suggests that merely inhibiting either NHEJ or HR repair pathways may not effectively resolve the issue of radioresistance in residual tumor cells. Consequently, this study opted to inhibit the EGFR pathway to suppress the NHEJ repair mechanism and the NF-κB pathway to inhibit the HR repair mechanism, as both pathways also influence cell survival, thereby significantly enhancing the radiotherapeutic killing effect on tumors. Immunohistochemical results demonstrated that, compared to cRGD-GR9G-(LLHH)3/siNC, cRGD-GR9G-(LLHH)3/siEGFR/siP65 significantly inhibited the expression of EGFR and P65 proteins. In the context of radiotherapy, cRGD-GR9G-(LLHH)3/siEGFR/siP65 reduced EGFR expression and thereby inhibited phospho-DNA-PKcs, suggesting suppression of the NHEJ repair mechanism; it also reduced P65 expression and thereby inhibited phospho-ATM, indicating suppression of the HR repair mechanism. The ultimate result was an increase in the expression levels of Phospho-H2A.X and a decrease in the number of KI67 positive cells in the group treated with cRGD-GR9G-(LLHH)3/siEGFR/siP65 combined with radiotherapy. This implies that cRGD-GR9G-(LLHH)3/siEGFR/siP65 may increase radiotherapy-induced DNA breaks while reducing proliferating cells.

Clinical therapeutic benefits were primarily based on the improvement of the quality of life and the extension of survival time in glioblastoma patients. As shown in Figure 6E, in the survival experiments of mice bearing glioblastoma, the combination of cRGD-GR9G-(LLHH)3/siEGFR/siP65 with radiotherapy significantly prolonged the survival of the mice. Tissue H&E staining and serum tests for ALT, AST, CREA, and UREA (Figure S4A and B) revealed that cRGD-GR9G-(LLHH)3/siEGFR/siP65 and various nanoparticles had no significant toxicity to the heart, liver, spleen, lungs, or kidneys. Assessment of immunogenicity through the detection of IFN-β, IL-6, and TNF-α levels showed that cRGD-GR9G-(LLHH)3/siEGFR/siP65 and the various nanoparticles exhibited no detectable immunogenicity (Figure S4C). In summary, these results suggested that cRGD-GR9G-(LLHH)3/siEGFR/siP65 has potential as an anti-glioblastoma agent and can significantly enhance the efficacy of radiotherapy without evident toxic side effects.

glioblastoma-bearing mice were in a moribund state and dying frequently, they were euthanized, and the whole tumor-bearing brain tissue was isolated for histology and stained with H&E. (**D**) EGFR, RELA/P65, Phospho-DNA-PKcs, Phospho-ATM, Phospho-H2A.X and Ki67 in orthotopic U87MG-Luc glioblastoma tissues were detected by immunohistochemical staining. The EGFR and RELA/P65 protein expression levels were assessed by determining the mean optical density (IOD/area). Ki67 antibody staining was used to identify proliferative cells in the tumor, and the results were reported as the percentage of ki67 positive cells over the total cells. Additionally, cells with an activated NHEJ repair pathway were stained with Phospho-DNA-PKcs, and the results were reported as the percentage of Phospho-DNA-PKcs positive cells over the total cells. Finally, cells with an activated HR repair pathway were stained with Phospho-ATM, and the results were reported as the percentage of Phospho-ATM positive cells over the total cells. (**E**) The survival curve of mice in all groups. (Positive cells were showing brown. Bar =500 μm or 50 μm).

Discussion

The quest to enhance the radiosensitivity of GBM while mitigating damage to healthy tissue has been a formidable challenge in neuro-oncology. Our study presents a novel approach that leverages the specificity of RNA interference via a targeted nanoparticle delivery system, providing a promising strategy to overcome radioresistance in GBM.

Nanoparticle Design and Functionalization

The design of our nanoparticles was a critical element in achieving successful gene silencing. Our self-assembled polymeric nanoparticles, formed through interactions like electrostatic adsorption and hydrogen bonding between siRNA molecules and oligopeptides, boast biocompatibility, biodegradability, targeting ability, low cost, and easy preparation.[25] Our findings demonstrate the efficacy of cRGD-GR9G-(LLHH)3 nanoparticles in specifically targeting and silencing EGFR and P65 genes, which are key in the radioresistance of GBM. The innovative design of these nanoparticles is crucial for their function. Under physiological conditions (pH 7.4), the (LLHH)3 motif stabilizes the nanoparticle core through hydrogen bonding and hydrophobic interactions, ensuring biocompatibility and stability in the bloodstream.[40] This design prevents premature siRNA release, reducing potential non-target cytotoxicity. Conversely, in the acidic endosomal environment of cancer cells, the pH-responsive (LLHH)3 motif triggers endosomal membrane disruption, releasing siRNA into the cytoplasm for targeted gene silencing.[28,40] Our circular dichroism spectra, intracellular distribution, hemolysis, and toxicity results further validate these mechanisms. Together, these features ensure the nanoparticles' targeted release mechanism confines the gene silencing effect to tumor cells, boosting therapeutic efficacy while minimizing side effects. The 9-arginine oligopeptide (R9) forms a weakly positive surface on the nanoparticle by interacting with negatively charged siRNA.[41] Additionally, peripheral PEG enhances hydrophilicity and tissue compatibility, preventing nanoparticle aggregation, prolonging circulation, and reducing toxicity.[41] By means of this, the peptide and siRNA assembled into spherical nanoparticles with c(RGDfk)s displayed on their surface for the targeting of αvβ3 receptors on neovascular endothelial cells and glioblastoma cells.[32,33] This research introduces a nano delivery system based on a stimuli-responsive peptide (cRGD-GR9G-(LLHH)3) for efficient siEGFR and siP65 delivery. The nanoparticles are endocytosed by cells and released into the cytoplasm due to the membrane-disrupting effect of the (LLHH)3 structure in the endosomal environment. This clever design addresses a common hurdle in nanoparticle-mediated gene delivery, where endosomal entrapment often leads to degradation of the therapeutic nucleic acids before reaching their target.

The BBTB poses another significant obstacle for therapeutic delivery to GBM.[29] Our nanoparticles utilized cRGD peptides to target αvβ3 integrins, which are overexpressed in GBM cells and neovascular endothelial cells within the brain tumor environment. This targeting strategy facilitated the crossing of the BBTB and preferential accumulation of nanoparticles within the tumor site, as confirmed by our in vivo imaging studies. This targeted approach not only enhances the concentration of therapeutic agents in the tumor but also reduces systemic exposure and potential side effects, a critical consideration in translational medicine.

Radiosensitization Through Targeted Gene Silencing

Our data reveal that cRGD-GR9G-(LLHH)3/siEGFR/siP65 nanoparticles are proficient in delivering siRNA that specifically targets EGFR and P65, key genes associated with the radioresistance of GBM. Implementing this dual gene silencing approach led to a substantial enhancement in radiosensitivity, indicated by increased DNA damage, diminished cell viability, and escalated apoptosis in vitro. This aligns with prior research that has pinpointed the EGFR and NF-κB pathways as essential for the repair of DNA damage and the survival of cancer cells.[13,14] Radiation therapy is known to induce the EGFR/PI3K/Akt signaling pathway independently of ligands, which in turn promotes NHEJ repair of DSBs by upregulating DNA-PK transcription and its activation through phosphorylation.[12,13] Additionally, recurrent irradiation can aberrantly activate the NF-κB signaling pathway, leading to HR repair in GBM, thereby contributing to radiation resistance.[14–16] By simultaneously inhibiting both pathways, our strategy effectively blocks the primary mechanisms of GBM radioresistance and promotes the accumulation of lethal DNA damage by concurrently hindering NHEJ and HR repair processes, as confirmed by our mechanistic study results, thereby significantly enhancing the therapeutic effect of radiotherapy.

The clinical implications of our findings are significant. The ability to sensitize GBM to radiotherapy could potentially extend patient survival and improve quality of life, as suggested by our in vivo studies showing prolonged survival in mice treated with the cRGD-GR9G-(LLHH)3/siEGFR/siP65 nanoparticles in combination with radiotherapy. Future clinical trials will be necessary to validate these results in humans and to further refine the dosing and administration schedule for optimal therapeutic outcomes.

While our study provides compelling evidence for the potential of RNAi-based radiosensitization in GBM, there are limitations to consider. The complexity of GBM genetic landscape means that resistance mechanisms may vary between patients, necessitating personalized approaches to therapy. Additionally, the long-term effects and potential immunogenicity of repeated nanoparticle administration remain to be fully elucidated. Future research should focus on the identification of biomarkers to predict response to RNAi-based radiosensitization and the development of combination therapies that could include chemotherapy, immunotherapy, or other targeted agents.

Conclusion

In conclusion, our study underscores the potential of using a targeted nanoparticle delivery system for RNAi therapy as a radiosensitizer in GBM treatment. By designing nanoparticles that can effectively navigate physiological barriers, specifically deliver siRNA to tumor cells, and facilitate endosomal escape, we have demonstrated a significant improvement in radiotherapy outcomes. This approach holds promise for enhancing the precision and efficacy of GBM treatment, paving the way for more successful clinical interventions in this challenging field.

Acknowledgments

This work was supported by the National Natural Science Foundation of China (Grant No. 82003210, No. 82373516), GuangDong Basic and Applied Basic Research Foundation (Grant No.2020A1515110183, No.2022A1515220136 and No. 2024A1515010830), Key Clinical Technology of Guangzhou (2019ZD17), Guangzhou key medical discipline construction project fund, Medical Scientific Research Foundation of Guangdong Province, China (A2023319),and Plan on enhancing scientific research in Guangzhou medical university (GMUCR2024-01019). Bohong Cen, Jian Zhang, and Xinghua Pan are co first authors.

Disclosure

The authors report no conflicts of interest in this work.

References

1. Ostrom QT, Price M, Neff C, et al. CBTRUS statistical report: primary brain and other central nervous system tumors diagnosed in the United States in 2016–2020. *Neuro Oncol*. 2023;25(12 Suppl 2):iv1–iv99. doi:10.1093/neuonc/noad149
2. Brennan CW, Verhaak RG, McKenna A, et al. The somatic genomic landscape of glioblastoma. *Cell*. 2013;155(2):462–477. doi:10.1016/j.cell.2013.09.034
3. Sulman EP, Ismaila N, Armstrong TS, et al. Radiation therapy for glioblastoma: American Society of Clinical oncology clinical practice guideline endorsement of the American Society for Radiation Oncology guideline. *J Clin Oncol*. 2017;35(3):361–369. doi:10.1200/JCO.2016.70.7562
4. Erasimus H, Gobin M, Niclou S, Van Dyck E. DNA repair mechanisms and their clinical impact in glioblastoma. *Mutat Res Rev Mutat Res*. 2016;769:19–35. doi:10.1016/j.mrrev.2016.05.005
5. Schaue D, McBride WH. Opportunities and challenges of radiotherapy for treating cancer. *Nat Rev Clin Oncol*. 2015;12(9):527–540. doi:10.1038/nrclinonc.2015.120
6. Ali MY, Oliva CR, Noman A, et al. Radioresistance in glioblastoma and the development of radiosensitizers. *Cancers*. 2020;12(9):2511. doi:10.3390/cancers12092511
7. Gujar AD, Le S, Mao DD, et al. An NAD+-dependent transcriptional program governs self-renewal and radiation resistance in glioblastoma. *Proc Natl Acad Sci U S A*. 2016;113(51):E8247–E8256. doi:10.1073/pnas.1610921114
8. Huang RX, Zhou PK. DNA damage response signaling pathways and targets for radiotherapy sensitization in cancer. *Signal Transduct Target Ther*. 2020;5(1):60. doi:10.1038/s41392-020-0150-x
9. O'Connor MJ. Targeting the DNA damage response in cancer. *Mol Cell*. 2015;60(4):547–560. doi:10.1016/j.molcel.2015.10.040
10. Blackford AN, Jackson SP. ATM, ATR, and DNA-PK: the trinity at the heart of the DNA damage response. *Mol Cell*. 2017;66(6):801–817. doi:10.1016/j.molcel.2017.05.015
11. Bao S, Wu Q, McLendon RE, et al. Glioma stem cells promote radioresistance by preferential activation of the DNA damage response. *Nature*. 2006;444(7120):756–760. doi:10.1038/nature05236
12. Westphal M, Maire CL, Lamszus K. EGFR as a target for glioblastoma treatment: an unfulfilled promise. *CNS Drugs*. 2017;31(9):723–735. doi:10.1007/s40263-017-0456-6

13. Debucquoy A, Machiels JP, McBride WH, Haustermans K. Integration of epidermal growth factor receptor inhibitors with preoperative chemoradiation. *Clin Cancer Res*. 2010;16(10):2709–2714. doi:10.1158/1078-0432.CCR-09-1622
14. McCool KW, Miyamoto S. DNA damage-dependent NF-kappaB activation: NEMO turns nuclear signaling inside out. *Immunol Rev*. 2012;246 (1):311–326. doi:10.1111/j.1600-065X.2012.01101.x
15. Bhat K, Balasubramaniyan V, Vaillant B, et al. Mesenchymal differentiation mediated by NF-kappaB promotes radiation resistance in glioblastoma. *Cancer Cell*. 2013;24(3):331–346. doi:10.1016/j.ccr.2013.08.001
16. Volcic M, Karl S, Baumann B, et al. NF-kappaB regulates DNA double-strand break repair in conjunction with BRCA1-CtIP complexes. *Nucleic Acids Res*. 2012;40(1):181–195. doi:10.1093/nar/gkr687
17. Wang R, Peng S, Zhang X, et al. Inhibition of NF-kappaB improves sensitivity to irradiation and EGFR-TKIs and decreases irradiation-induced lung toxicity. *Int J Cancer*. 2019;144(1):200–209. doi:10.1002/ijc.31907
18. Barata P, Sood AK, Hong DS. RNA-targeted therapeutics in cancer clinical trials: current status and future directions. *Cancer Treat Rev*. 2016;50:35–47. doi:10.1016/j.ctrv.2016.08.004
19. Wilson RC, Doudna JA. Molecular mechanisms of RNA interference. *Annu Rev Biophys*. 2013;42:217–239. doi:10.1146/annurev-biophys-083012-130404
20. Rüger J, Ioannou S, Castanotto D, Stein CA. Oligonucleotides to the (Gene) rescue: FDA approvals 2017–2019. *Trends Pharmacol Sci*. 2020;41 (1):27–41. doi:10.1016/j.tips.2019.10.009
21. Khvorova A, Watts JK. The chemical evolution of oligonucleotide therapies of clinical utility. *Nat Biotechnol*. 2017;35(3):238–248. doi:10.1038/nbt.3765
22. Collins I, Workman P. New approaches to molecular cancer therapeutics. *Nat Chem Biol*. 2006;2(12):689–700. doi:10.1038/nchembio840
23. Dowdy SF. Overcoming cellular barriers for RNA therapeutics. *Nat Biotechnol*. 2017;35(3):222–229. doi:10.1038/nbt.3802
24. Hu B, Zhong L, Weng Y, et al. Therapeutic siRNA: state of the art. *Signal Transduct Target Ther*. 2020;5(1):1–25. doi:10.1038/s41392-019-0089-y
25. Boisguerin P, Konate K, Josse E, Vives E, Deshayes S. Peptide-based nanoparticles for therapeutic nucleic acid delivery. *Biomedicines*. 2021;9 (5):583. doi:10.3390/biomedicines9050583
26. Degors I, Wang C, Rehman ZU, Zuhorn IS. Carriers break barriers in drug delivery: endocytosis and endosomal escape of gene delivery vectors. *Acc Chem Res*. 2019;52(7):1750–1760. doi:10.1021/acs.accounts.9b00177
27. Ismail M, Wang Y, Li Y, Liu J, Zheng M, Zou Y. Stimuli-responsive polymeric nanocarriers accelerate on-demand drug release to combat glioblastoma. *Biomacromolecules*. 2024;25:6250–6282. doi:10.1021/acs.biomac.4c00722
28. Bird GH, Mazzola E, Opoku-Nsiah K, et al. Biophysical determinants for cellular uptake of hydrocarbon-stapled peptide helices. *Nat Chem Biol*. 2016;12(10):845–852. doi:10.1038/nchembio.2153
29. van Tellingen O, Yetkin-Arik B, de Gooijer MC, Wesseling P, Wurdinger T, de Vries HE. Overcoming the blood-brain tumor barrier for effective glioblastoma treatment. *Drug Resist Updat*. 2015;19:1–12. doi:10.1016/j.drup.2015.02.002
30. Muhammad P, Hanif S, Li J, et al. Carbon dots supported single Fe atom nanozyme for drug-resistant glioblastoma therapy by activating autophagy-lysosome pathway. *Nano Today*. 2022;45:101530. doi:10.1016/j.nantod.2022.101530
31. Wang N, Jain RK, Batchelor TT. New directions in anti-angiogenic therapy for glioblastoma. *Neurotherapeutics*. 2017;14(2):321–332. doi:10.1007/s13311-016-0510-y
32. Chen C, Duan Z, Yuan Y, et al. Peptide-22 and cyclic RGD functionalized liposomes for glioma targeting drug delivery overcoming BBB and BBTB. *ACS Appl Mater Interfaces*. 2017;9(7):5864–5873. doi:10.1021/acsami.6b15831
33. Cen B, Wei Y, Huang W, et al. An efficient bivalent cyclic RGD-PIK3CB siRNA conjugate for specific targeted therapy against glioblastoma in vitro and in vivo. *Mol Ther Nucleic Acids*. 2018;13:220–232. doi:10.1016/j.omtn.2018.09.002
34. Rehman FU, Liu Y, Yang Q, et al. Heme Oxygenase-1 targeting exosomes for temozolomide resistant glioblastoma synergistic therapy. *J Control Release*. 2022;345:696–708. doi:10.1016/j.jconrel.2022.03.036
35. Ismail M, Yang W, Li Y, et al. Targeted liposomes for combined delivery of artesunate and temozolomide to resistant glioblastoma. *Biomaterials*. 2022;287:121608. doi:10.1016/j.biomaterials.2022.121608
36. Zhang Y, Sun X, Huang M, Ke Y, Wang J, Liu X. A novel bispecific immunotoxin delivered by human bone marrow-derived mesenchymal stem cells to target blood vessels and vasculogenic mimicry of malignant gliomas. *Drug Des Devel Ther*. 2015;9:2947–2959. doi:10.2147/DDDT.S79475
37. Ozawa T, James CD. Establishing intracranial brain tumor xenografts with subsequent analysis of tumor growth and response to therapy using bioluminescence imaging. *J Vis Exp*. 2010;41(41). doi:10.3791/1986
38. Richard JP, Melikov K, Vives E, et al. Cell-penetrating peptides. A reevaluation of the mechanism of cellular uptake. *J Biol Chem*. 2003;278 (1):585–590. doi:10.1074/jbc.M209548200
39. Wiradharma N, Khoe U, Hauser CA, Seow SV, Zhang S, Yang YY. Synthetic cationic amphiphilic alpha-helical peptides as antimicrobial agents. *Biomaterials*. 2011;32(8):2204–2212. doi:10.1016/j.biomaterials.2010.11.054
40. He J, Xu S, Mixson AJ. The multifaceted histidine-based carriers for nucleic acid delivery: advances and challenges. *Pharmaceutics*. 2020;12 (8):774. doi:10.3390/pharmaceutics12080774
41. Raftery RM, Walsh DP, Castano IM, et al. Delivering nucleic-acid based nanomedicines on biomaterial scaffolds for orthopedic tissue repair: challenges, progress and future perspectives. *Adv Mater*. 2016;28(27):5447–5469. doi:10.1002/adma.201505088
42. Longmire MR, Ogawa M, Choyke PL, Kobayashi H. Biologically optimized nanosized molecules and particles: more than just size. *Bioconjugate Chem*. 2011;22(6):993–1000. doi:10.1021/bc200111p
43. Forest V, Pourchez J. Preferential binding of positive nanoparticles on cell membranes is due to electrostatic interactions: a too simplistic explanation that does not take into account the nanoparticle protein Corona. *Mater Sci Eng C Mater Biol Appl*. 2017;70(Pt 1):889–896. doi:10.1016/j.msec.2016.09.016